Correlation between OCVD carrier lifetime vs temperature measurements and reverse recovery behavior of the body diode of SiC power MOSFETs

Correlation between OCVD carrier lifetime vs temperature measurements and reverse recovery behavior of the body diode of SiC power MOSFETs

S. Sapienza, G. Sozzi*, D. Santoro, P. Cova, N. Delmonte, G. Verrini and G. Chiorboli
Department of Engineering and Architecture, University of Parma, Parco Area delle Scienze 181/a, 43124, Parma, Italy

Abstract
The reverse recovery behavior of SiC MOSFET body diode is of great importance in power application, where these devices are used in a wide range of operating temperatures. The carrier lifetime in the drift region varies with temperature, and it heavily affects the tailoring of the reverse recovery current, opening reliability issues related to the reverse recovery voltage amplitude and to possible anomalous voltage oscillations during the recovery. From the users' point of view, it would be useful to have a simple technique able to give predictive information about the body diode reverse recovery behavior of commercial devices over the whole range of working temperatures. An experimental-simulation approach is presented in this paper to correlate the carrier lifetime measured by simple OCVD measurements versus temperature with the reverse recovery behavior of the body diode, that can be useful at the design stage of power converters. Simulations of the body-diode reverse-recovery are performed for a wide range of carrier lifetimes. This allows to estimate the effect of changes of carrier lifetime with temperature on the body-diode switching transients. Preliminary results obtained with a 1700V/5A commercial MOSFET are shown.

1. Introduction

Wide-bandgap semiconductors gained market rapidly in the last decade, especially for power applications. High voltage Silicon Carbide (SiC) MOSFETs demonstrated superior performance in term of switching characteristics and on-state resistance [1]. These properties, combined with the ability to work optimally at high temperatures, makes them now competitive compared to silicon devices. Nowadays, their cost is no longer a limitation to their massive diffusion, but their reliability is not yet proven to be at the same level of the silicon counterparts.

Due to their high speed, one of the most critical reliability issues is related to the switching characteristic of the body diode [2-6]. Indeed, due to the high current slope during the recovery phase of the transient, and to the presence of circuit parasitic inductances, high over-voltages and possible dangerous self-oscillations may arise. The carrier lifetime in the drift region is the key parameter in determining the softness [7] of the device, and many techniques were used to improve its control, from ions implantation to electrons or protons irradiation [8].

SiC devices are often used in a wide range of operating temperatures [1] and the temperature dependence of the carrier lifetime [9] may induce large modification in the switching characteristic of the body diode. From the point of view of the MOSFET's user it is important to be able to decide if the body diode can be exploited in a specific application. Unfortunately, the measurement of the reverse recovery behavior at different switching conditions and different operating temperatures is not an easy task. For this reason, in this work it is demonstrated the possibility to exploit a simple carrier lifetime measurement method to predict the temperature evolution of the reverse recovery behavior of the body diode.

The simplest method to measure the carrier lifetime in PiN diodes is the Open Circuit Voltage Decay (OCVD) technique [10], which will be described in Section 2. OCVD measurements are performed on the body diode of a commercial MOSFET at various temperatures. Numerical simulations of inductive reverse recovery were also performed in order to evaluate the impact of the carrier lifetime variation with temperature on the switching characteristics of the diode; to this purpose, a wide range of carrier lifetimes was investigated.

Section 2 describes the characterization and analytical methods used in this work. Section 3 presents and discusses the results of measurements and simulations. In Section 4 the conclusions are drawn.

2. Methods and materials

In this section, the methods used for static and switching characterizations of SiC MOSFET's body diode are described. Moreover, qualitative Reverse-Recovery (RR) simulations were carried out with the software Synopsys Sentaurus TCAD [11] to analyze the switching properties of devices with different carrier lifetimes.

The measurements were carried out on a commercial

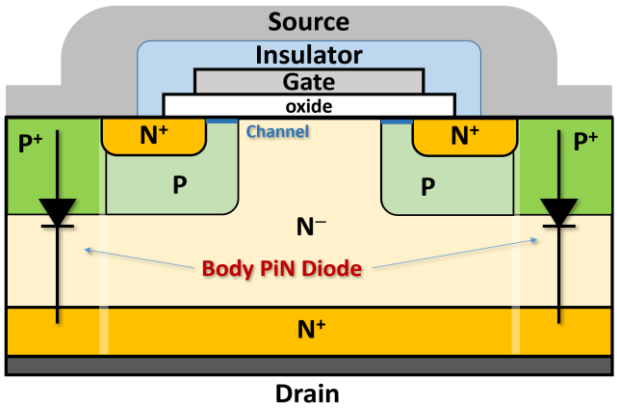

Fig. 1. Schematic cross section of a typical SiC power MOSFET structure.

* Corresponding author. giovanna.sozzi@unipr.it
Tel: +39 0521 906044; Fax: +39 0521 905822

C2M1000170D SiC MOSFET from Cree Inc. rated at 1700V/5A.

A schematic cross section of a SiC vertical n-channel power MOSFET with a planar gate structure is shown in Fig. 1.

The body diode is the intrinsic vertical PiN diode, through the P^+ well, the N^- drift region and the N^+ drain region. It can be exploited to conduct currents when inductive loads force the SiC power MOSFET to operate, as a bi-directional switch, in the third quadrant of the I-V plane, avoiding the use of an external diode.

2.1 Temperature-dependent current-voltage (IVT) static measurements

Temperature-dependent current-voltage static measurements in forward-bias region (i.e., shorting the gate and source of the MOSFET) were carried out applying a pulsed technique to avoid self-heating of the body diode during the curve tracing. To do this, the device was biased with the circuit of Fig. 2, a bipolar pulser made with a half bridge as proposed in [12]. With the chosen device, self-heating has negligible effect if the pulse duration T_P is lower than 200 µs. The pulsed biasing of the body diode, i.e. the Device Under Test (DUT), is obtained with a half bridge driven by a low power pulse generator (e.g., a Philips

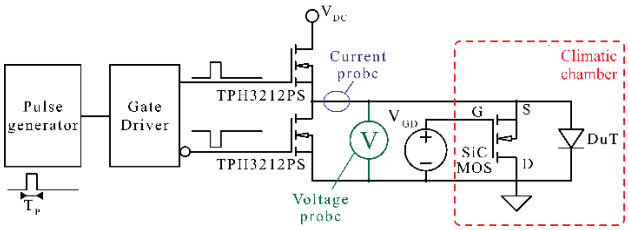

Fig. 2. Schematic diagram of the IVT measurement setup.

PM5781 programmable generator).

The half bridge is made by GaN transistors TPH3212PS from Transphorm Inc. When the positive pulse is applied to the GaN FET connected to V_{DC} (then the lower GaN FET of the half bridge is off) the voltage between the anode and the cathode of the DUT is positive. During T_P the diode current and voltage (V_{DC} minus the voltage drop across the upper on-state GaN FET) are measured with an oscilloscope. In this case, a Tektronix DPO7254 oscilloscope was used, sensing the current

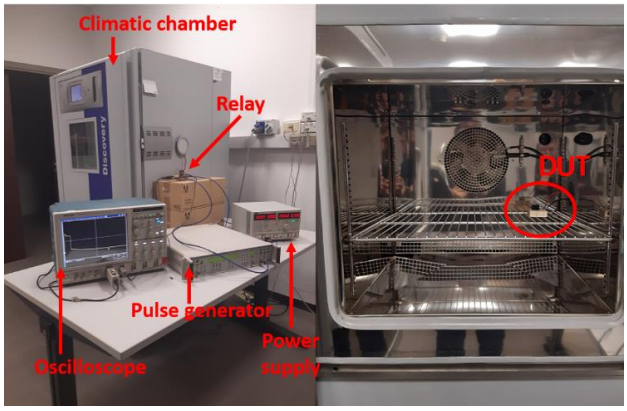

Fig. 3. Experimental setup used for IVT and OCVD measurements: (left) whole test bench; (right) DUT inside the climatic chamber.

with a Tektronix TCP0030 probe and the voltage with a Tektronix P6139A passive probe. By varying V_{DC} at every pulse, it is possible to trace the IV curve in the forward-bias region. In all measurements the gate-drain bias voltage, V_{GD}, was kept fixed at -10 V to avoid the parasitic MOSFET current in addition to the PiN current path [13].

To keep the temperature fixed at a known value, the DUT is placed in a climatic chamber (Fig. 3). In the case study presented here, IVT curves have been measured in the temperature range 298-448 K, with T_P = 100 µs.

2.2 OCVD measurements versus temperature

To estimate the carrier's lifetime in the drift region, the OCVD technique has been used [14,15], which can be very useful and simpler to implement [16], compared to the reverse recovery one and regarding the available electrical techniques. Optical measurements are not useful with commercial devices, because it would be necessary to bias the device without the package.

In the OCVD technique, the diode is firstly biased in high-injection condition by a DC voltage supply, V_{DC}, which is suddenly disconnected from the diode by the fast opening of a mercury relay controlled by a pulse generator (Fig. 4). The subsequent voltage decay, V(t), is recorded and the carrier lifetime in high-injection condition, or high-level lifetime, $\tau_{HL,OCVD}$, is extracted from the slope of the linear trait of the voltage decay as:

$$\tau_{HL,OCVD} = -2v_{th}\frac{1}{dV(t)/dt} \quad (1)$$

where v_{th} is the thermal voltage.

The test bench set up for OCVD measurements, schematically shown in Fig. 4, includes a TTi QL355TP power supply for DC voltage with a maximum current of 5 A. A 200-1-A-5/6D mercury wetted relay from Pickering has been used to avoid the bounce effects during switching [17]. The most important features of this mercury relay are the power rating of 50 W, the maximum operating current of 3 A, a very high open circuit resistance (> 10^{12} Ω), and a turn-on time of the order of 10 ns.

To generate the pulse, a Philips PM5781 programmable pulse generator was used.

During a measurement, the DUT was kept in the climatic chamber at a fixed and well-known temperature.

Temperature-dependent OCVD measurements were carried out in the range of 298-448 K, with bias voltages, V_{DC}, giving a current of 3 A. A resistance of 1 MΩ was added in parallel to the DUT in order to compensate for the observed capacitance-

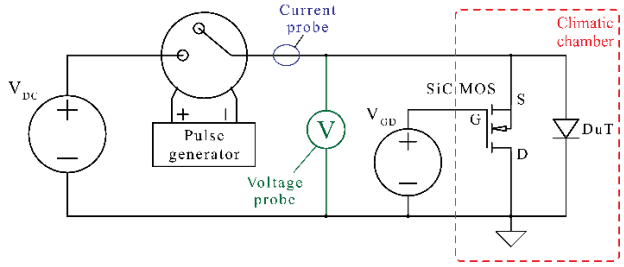

Fig. 4. Schematic diagram of the OCVD measurement setup.

controlled behavior of the voltage decay, as suggest by Green [18].

The relay is closed by a pulse with duration of 1 ms and amplitude of 5 V, which is the minimum voltage to activate the relay coil.

To acquire the voltage decay curve and measure the current level, the same probes and oscilloscope of the IV measurements were used.

3 Simulations

A numerical model of a possible SiC body diode was realized with the commercial Synopsys Sentaurus TCAD code [11]. Since no details are known about the MOSFET structure (i.e., layer thicknesses, doping levels, well dimensions, etc.), we modeled a generic 4H-SiC diode with the aim to describe, even only qualitatively, the possible effect of the variation of carrier lifetime with temperature on the body diode switching behavior.

We considered a drift region of 20 μm with a doping level of $1 \cdot 10^{16}$ cm^{-3}, corresponding to a theoretical BV of about 1800 V. The diode behavior is described by the Poisson, electron and hole continuity, and drift-diffusion equations. An additional model accounting for the incomplete ionization of dopants in 4H-SiC [19] is included in the diode model. The dependence of hole and electron mobilities on doping is described by the empirical relation of Caughey–Thomas with parameters for SiC taken from [20]. The fundamental parameters of 4H-SiC and additional details about the diode simulation can be found in our previous work [21].

Trap-assisted recombination follows the Shockley–Read–Hall statistics: we considered same electron and hole lifetimes, $\tau_c = \tau_e = \tau_h$, with values ranging between 15 ns and 50 μs.

The value of carrier lifetime in the voltage-blocking layer is critical as it influences the device on-state resistance as well as the turn-off of the body diode.

The main lifetime-killer defect in 4H-SiC has been identified with $Z_{1/2}$ center by several authors [22,23], and it is systematically found in 4H-SiC n-doped epi-layers [24,25]. It originates from the carbon vacancy [26,27] whose density can be influenced by several factors, as the temperature of n-doped epi-layer growth [28], the annealing processing following the ion-implantation step [29], or the sample thermal treatments [30].

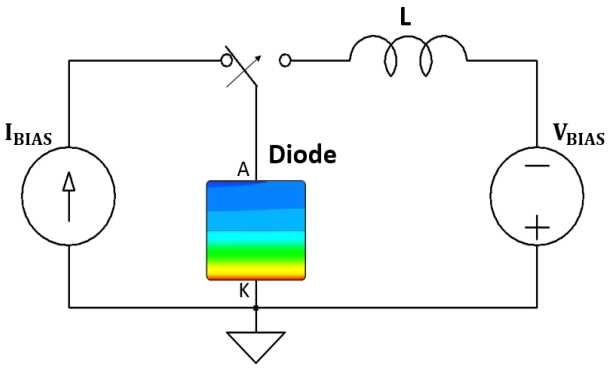

Fig. 5. Mixed-mode circuit used in the numerical simulation of diode reverse recovery. The diode model and circuit parameters are described in the text.

It has been also shown [31] that in the case of a very low carbon - vacancy density, whose exact value also depends on the thickness of the epi-layer, the carrier lifetime is no longer limited by recombination at these defects.

The diode reverse recovery is simulated by introducing the 3D diode model into the mixed-mode circuit shown in Fig. 5, where the remaining components are described by spice-like compact models: the diode is firstly biased in forward condition by a current of 3 A (the same level of measurements), afterwards it is switched at a forward turn-off di/dt of 1200 A/μs, the same slope used as standard condition in the SiC MOSFET datasheet.

We repeated the simulation of the diode reverse recovery for carrier lifetimes, τ_c, covering a wide range of values, namely 15 ns, 50 ns, 150 ns, 500 ns, 1.5 μs, 5 μs, 15 μs, 50 μs. All simulations were performed at RT (300 K).

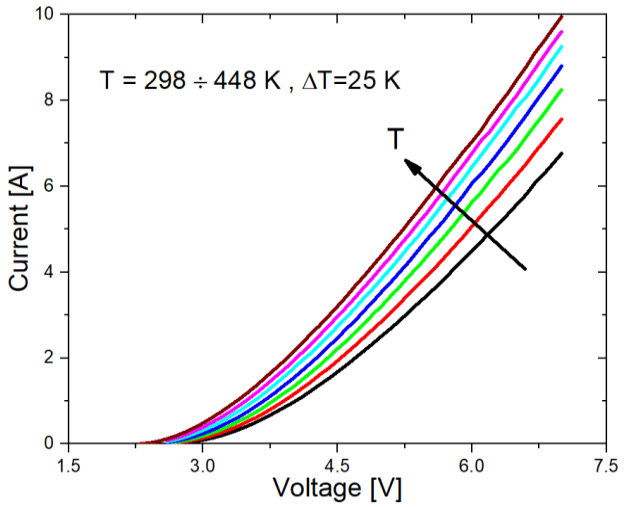

Fig. 6. Measured body-diode IVT curves, in the temperature range of 298-448 K, with steps ΔT = 25 K and V_{GD} = -10 V.

3. Results and discussion

Fig. 6 shows the results of the temperature dependent IV static measurements, carried out in the range 298 - 448 K, with a step of 25 K.

The IVT curves were acquired up to 7 V, where it could be observed the maximum current variation. The average current variation spans from 10 % to 3 %, increasing temperature, between each adjacent curve.

The measured OCVD curves are shown in Fig. 7a for different temperatures; the inset highlights the corresponding current transients. The considerable voltage drop of about 2 V appearing at the time of 0.19 ms, corresponding to the relay opening instant, is due to the device series resistance.

After a while from the relay opening, a linear trait of approximate duration T_{int} appears in the voltage decay as visible in the enlargement of Fig. 7b, which allows to extract the lifetime $\tau_{HI,OCVD}$.

$\tau_{HI,OCVD}$ is calculated with (1) from the slope of $V(t)$ obtained by the linear interpolation of $V(t)$ over the time window of duration T_{int}. The procedure is then repeated for all the curves

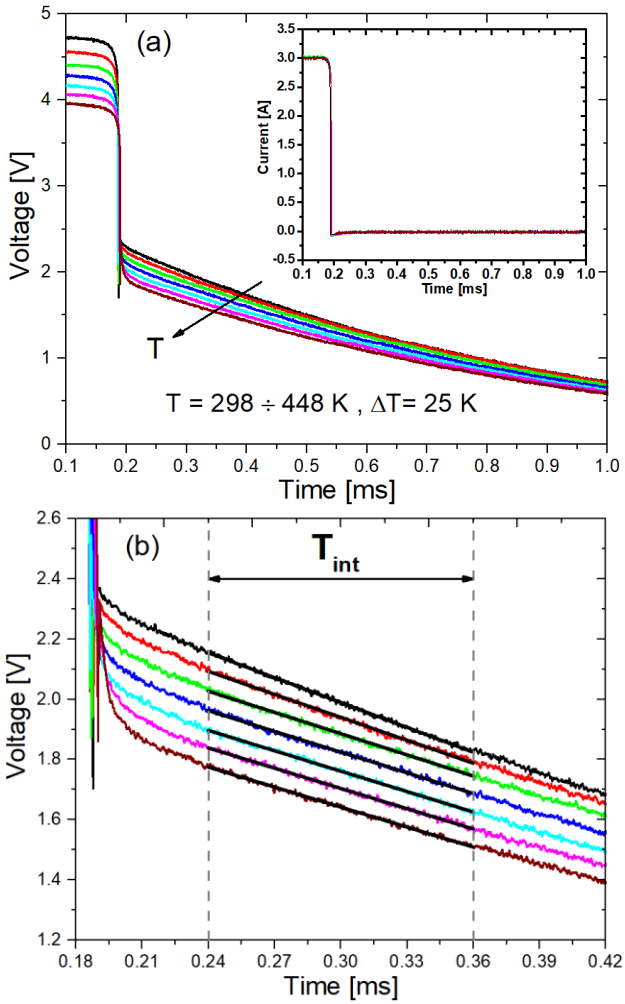

Fig. 7. a) Measured open circuit voltage decay, $V(t)$ at different ambient temperature for a bias current of 3 A (shown in the inset) and V_{GD} = -10 V. b) Enlargement of $V(t)$ in the time window T_{int}, showing the linear trait from which the lifetime is extracted by (1) from the voltage decay.

measured at different temperatures.

The measured temperature-dependent lifetimes are shown in Fig. 8 in a log-log scale: the lifetime ranges from about 19 µs to about 35 µs.

Recently in [32], the correlation between the carbon vacancy density and the carrier lifetime has been investigated by theoretical calculation with a model based on the rate of carrier recombination via the $Z_{1/2}$ center that is originated from the carbon-vacancy. It has been found that, due to the characteristics of the two acceptor levels associated with the $Z_{1/2}$ center, the carrier lifetime under high-injection condition is about ten times higher than in low-injection regime.

A law was also proposed describing the correlation between the high-level lifetime, τ_{HL}, and the carbon vacancy density, N_{CV}:

$$\tau_{HL} = \frac{1.5 \cdot 10^{13}}{N_{CV}\ (cm^{-3})}\,\mu s \qquad (2)$$

From the proposed law, using the measured $\tau_{HI,OCVD}$ = 19 µs at room-temperature, a carbon-vacancy density $N_{CV} = 7.9 \cdot 10^{11}$ cm^{-3} can be calculated for the studied device.

In addition, it has been also observed in [31,32] that the dependence of t_{HL} on N_{CV} described by (2) no longer agrees with the experimental data for N_{CV} values lower than $N_{CV,MIN} = 1 - 3 \cdot 10^{11}$ cm^{-3}, indicating that other recombination centers are controlling the carrier lifetime.

The $Z_{1/2}$ density can be reduced by appropriately treating the SiC either with thermal oxidation or with silicon or carbon ion implantation and subsequent annealing treatments [33].

Ichikava at al. measured carrier lifetime of 1.1 µs in as-growth 4H-SiC [34], that increases to 26.1 µs after thermal-oxidation at 1400°C of the epi-layer and to 33.1 µs after additional surface passivation treatments. Similarly, a high-level lifetime of 19.2 µs and bulk lifetime between 22–31 µs has been measured after treating different samples with Carbon implant followed by thermal annealing and passivation [35].

Based on these observations, we may speculate that the high measured lifetime of the studied device is compatible with a treated epi-layer and a reduced influence of surface recombination processes.

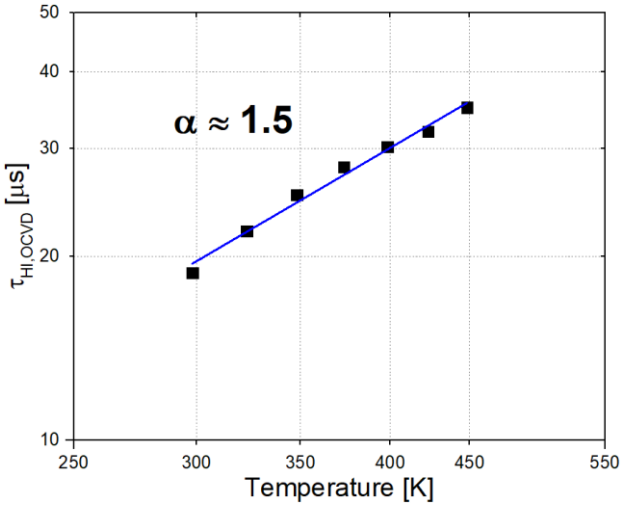

Fig. 8. Measured temperature dependent carrier lifetimes, τ, symbols, calculated from OCVD decay in log-log scale; the blue dashed line is data fitting using the power law dependence of carrier lifetime on temperature as defined by (4), and α is the extracted exponent.

3.1 Temperature-dependence of lifetime

The minority carrier lifetime, τ, in case of defect-assisted recombination, is related to the defect capture cross section, σ, the thermal velocity, v_{th}, varying with $T^{1/2}$ and the trap density, N_t:

$$\tau = \frac{1}{\sigma\, v_{th} N_t} \qquad (3)$$

The magnitude of the capture cross section and its dependence on temperature shall reflect the carrier recombination process through which the energy corresponding to the energy difference between the band and the defect level is transformed

into phonons. In particular, its temperature-dependence is a characteristic feature of the physical mechanism of carrier recombination in the impurity level.

In the case of high-injection levels, the lifetime asymptotically approaches a constant value referred to as the high-level lifetime that is the sum of the electron and hole minority carrier lifetime [36].

In order to verify the presence of a dominant thermally activated recombination process in the studied device, we thus investigated the possible mechanism at the origin of the measured lifetime, analyzing the experimental results in the light of the carrier lifetime model that has been developed for defect-assisted recombination process.

A power law dependence of lifetime on temperature (τ_0 is the lifetime at 300 K and T the temperature in K) can appear in Coulomb-attractive recombination centers [37,38]:

$$\tau = \tau_0 \left(\frac{T}{300\ K}\right)^{\alpha} \tag{4}$$

This phonon-assisted process is based on the assumption that a defect possesses excited levels, so that a carrier loses its energy by emitting one phonon every time it decays from an excited state to a less excited state of a defect. In this case, the related capture cross section decreases with temperature since the probability of carrier re-emission is larger at higher temperatures.

A value $\alpha \approx 2$ has been reported in [9], while values of about 1.9 and 1.2 can be inferred by data shown in [39] and [40], respectively.

By fitting the experimental data with (4) over the whole temperature range, a factor $\alpha = 1.5$ was extracted from the measured lifetimes of Fig. 8 (blue solid line): this implies (from (3)), the existence of a power law dependence of σ on T^{-2}, as expected for this recombination mechanism [38].

3.2 Diode reverse recovery simulation

The numerical simulations provide a convenient tool to analyze the impact of the observed changes in the carrier lifetime with temperature on the body diode switching behavior. In order to decouple the effect of lifetime variation with temperature from other temperature-dependent parameters that might affect the reverse recovery, we only change the carrier lifetime and fix the device ambient temperature at room-temperature. It is worth recalling here, that, while the performed OCVD measurements give an estimation of the high-level lifetime, the diode reverse-recovery behavior is mainly determined by the recombination minority carrier lifetime. As known, it is desirable to have a large high-level lifetime to maximize the conductivity of the drift region during current flow, and at the same time, to have a low minority carrier lifetime to speed up the removal of the excess minority carriers, resulting in faster device turning off.

Since the minority carrier lifetime, that is a fraction of the high-level lifetime, depends on many unknown parameters as the position of the defect energy level in the forbidden energy gap, the carrier injection level or the dopant concentration of semiconductor [36], we performed simulations of the diode reverse recovery over a wide range of minority carrier recombination lifetimes, τ_c (i.e., 15 ns $\leq \tau_c \leq$ 50 µs).

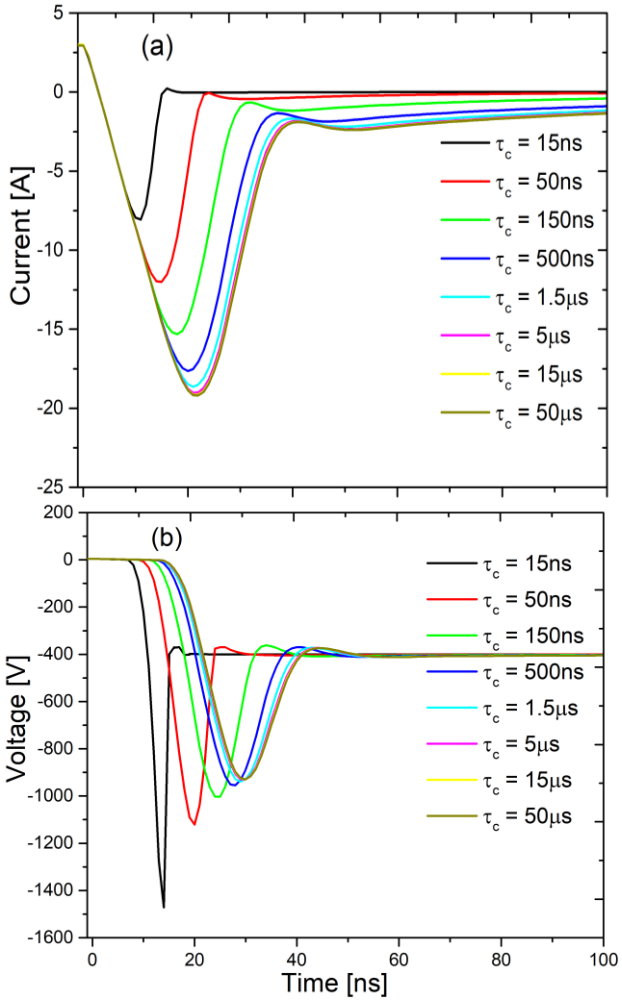

Fig. 9. Simulated reverse recovery transients; a) current and b) voltage, for different carrier lifetime τ_c.

The simulated current and voltage during the reverse recovery are shown in Fig. 9 for different τ_c; in all cases the body diode switches with a forward current of 3 A. As can be seen from Fig. 9a, the increase of carrier lifetime causes the peak reverse recovery current and related stored recovery charge (i.e., the integral of the triangle shaped reverse current), to increase, as expected.

Calling t_A the time between the zero crossing of the current and the peak reverse current, and t_B the time between the peak of the reverse current and the time where the current falls to a pre-defined low level (for instance 10% of the peak), the diode reverse recovery time, t_{RR}, can be expressed as $t_{RR} = t_A + t_B$. It can be observed in Fig. 9a, that both t_A and t_B, and thus t_{RR}, become larger for longer carrier lifetimes. It is thus important to evaluate the effect of this variation on the diode softness, usually defined as $S = t_B/t_A$. Since the shape of the reverse recovery current could also be very different from triangular, it is preferable to use another definition of the softness [7], which

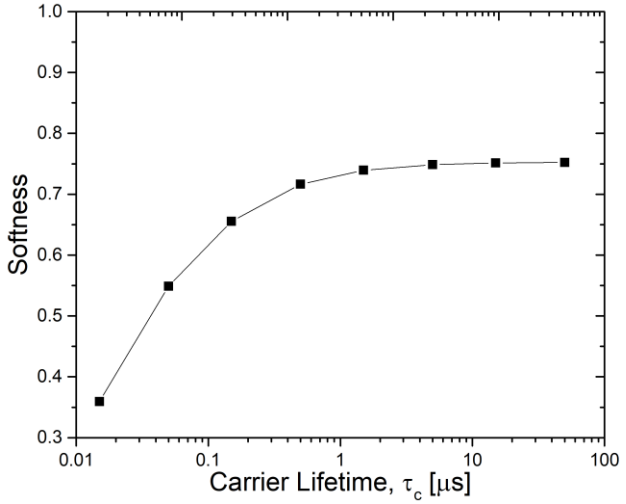

Fig. 10. Simulated diode softness, S, calculated from the curves in Fig. 9 with (5).

takes into account the maximum slope of the recovery current during t_B, which is responsible for the diode overvoltage peak:

$$S = \frac{|\mathrm{d}I_D/\mathrm{d}t|_{\mathrm{A}}}{|\mathrm{d}I_D/\mathrm{d}t|_{\mathrm{B(max)}}} \tag{5}$$

A hard switching behavior might cause unwanted and dangerous conditions, such as oscillation, increasing losses, false switching, and electromagnetic interference in the circuit [7], therefore it is important to relate the softness with the carrier lifetime. Fig. 10 depicts the diode softness versus the carrier lifetime calculated from the simulated reverse recovery curves of Fig. 9 with (5). *S* sharply increases for τ_c ranging between 15 ns and 150 ns, while it is almost constant for τ_c larger than 1.5 µs. A benefit of the increased *S* is the reduction of reverse recovery voltage peak, which drops from about 1470 V to 830 V for τ_c = 50 ns and 50 µs, respectively. In the case of the commercial MOSFETs taken as DUT in this work, the lifetime measured by OCVD is in the range of tens of µs, and does not change appreciably below 373 K.

For higher temperatures, it increases, and therefore we can expect a weak slowdown of the diode reverse recovery transient, and a decrease of the reverse voltage peak, with no anomalous behavior arising.

4. Conclusions

The carrier lifetime realistic temperature dependence is one of the most important parameter to know when dealing with bipolar device, as the body-diode of a MOSFET device, as it controls the diode switching behavior and can determine the onset of excessive voltage amplitudes or oscillations during the diode reverse recovery, posing reliability issues.

We measured the carrier lifetime in the drift region of a commercial SiC MOSFET by applying the OCVD method to the internal PiN body-diode. The measurements were repeated over a ambient temperature interval of 150 K, to trace the changes of the carrier lifetime due to self-heating in operating conditions. OCVD lifetime of 19 µs at room temperature has been measured. In the investigated temperature interval, the measured lifetime increases following a power-law dependence on temperature. An exponent of 1.5 was extracted from experimental data.

Possible changes in the body-diode reverse recovery behavior due to the variation of carrier lifetime with the device temperature were investigated through numerical simulations, showing a beneficial effect of the temperature increase on the body diode softness in the case of low minority carrier lifetimes.

The numerical simulations can give more specific insight into how the body diode behaves during the reverse recovery time if more information about the device physical structure are known.

However, we showed that, even in case of absolute absence of physical information on the device structure, simple OCVD measurements can be used to give indication about the temperature evolution of the switching behavior of the body diode. Therefore, OCVD can represent a useful technique to characterize the SiC MOSFET body diode, and then support the designer in the choice of the proper device for a specific application.

References

[1] L. F. S. Alves, P. Lefranc, P. Jeannin, and B. Sarrazin, "Review on SiC-MOSFET devices and associated gate drivers," in *2018 IEEE International Conference on Industrial Technology (ICIT)*, 2018, pp. 824–829.

[2] R. Bonyadi, O. Alatise, S. Jahdi, J. Hu, L. Evans, and P. A. Mawby, "Investigating the reliability of SiC MOSFET body diodes using Fourier series modelling," in *2014 IEEE Energy Conversion Congress and Exposition (ECCE)*, 2014, pp. 443–448.

[3] A. Fayyaz, G. Romano, and A. Castellazzi, "Microelectronics Reliability Body diode reliability investigation of SiC power MOSFETs," *Microelectron. Reliab.*, vol. 64, pp. 530–534, 2016.

[4] M. R. Ahmed, R. Todd, and A. J. Forsyth, "Switching performance of a SiC MOSFET body diode and SiC schottky diodes at different temperatures," in *2017 IEEE Energy Conversion Congress and Exposition (ECCE)*, 2017, pp. 5487–5494.

[5] "Reliability of SiC-MOSFETs." [Online]. Available: https://micro.rohm.com/en/techweb/knowledge/sic/s-sic/04-s-sic/6888.

[6] H. Li, J. Wang, N. Ren, H. Xu, and K. Sheng, "Investigation of 1200 V SiC MOSFETs' Surge Reliability," *Micromachines*, vol. 10, no. 7, 2019.

[7] P. Cova, R. Menozzi, and M. Portesine, "Experimental and numerical study of the recovery softness and overvoltage dependence on p–i–n diode design," *Microelectronics J.*, vol. 37, no. 5, pp. 409–416, 2006.

[8] P. Cova, R. Menozzi, M. Portesine, M. Bianconi, E. Gombia, and R. Mosca, "Experimental and numerical study of H+ irradiated p–i–n diodes for snubberless applications," *Solid. State. Electron.*, vol. 49, no. 2, pp. 183–191, 2005.

[9] A. Udal and E. Velmre, "Investigation of Charge Carrier Lifetime Temperature-Dependence in 4H-SiC Diodes," *Mater. Sci. Forum*, vol. 556–557, pp. 375–578, 2007.

[10] M. Derdouri, P. Leturcq, and A. Munoz-Yague, "A comparative study of methods of measuring carrier lifetime in p-i-n devices," *IEEE Trans. Electron Devices*, vol. 27, no. 11, pp. 2097–2101, Nov. 1980.

[11] "Synopsys Sentaurus TCAD." [Online]. Available: https://www.synopsys.com/.
[12] L. Svilainis, A. Chaziachmetovas, and V. Dumbrava, "Efficient high voltage pulser for piezoelectric air coupled transducer," *Ultrasonics*, vol. 53, no. 1, pp. 225–231, 2013.
[13] V. Pala *et al.*, "Physics of bipolar, unipolar and intermediate conduction modes in Silicon Carbide MOSFET body diodes," in *2016 28th International Symposium on Power Semiconductor Devices and ICs (ISPSD)*, 2016, pp. 227–230.
[14] S. R. Lederhandler and L. J. Giacoletto, "Measurement of Minority Carrier Lifetime and Surface Effects in Junction Devices," *Proc. IRE*, vol. 43, no. 4, pp. 477–483, 1955.
[15] H. Schlangenotto and W. Gerlach, "On the post-injection voltage decay of p-s-n rectifiers at high injection levels," *Solid State Electron.*, vol. 15, no. 4, pp. 393–402, 1972.
[16] G. Sozzi, M. Puzzanghera, G. Chiorboli, and R. Nipoti, "OCVD lifetime measurements on 4H-SiC bipolar planar diodes: Dependences on carrier injection and diode area," *IEEE Trans. Electron Devices*, vol. 64, no. 6, pp. 2572–2578, 2017.
[17] R. J. Bassett, "Observations on a method of determining the carrier lifetime in p+-v-n+ diodes," *Solid. State. Electron.*, vol. 12, no. 5, pp. 385–391, 1969.
[18] M. A. Green, "Minority carrier lifetimes using compensated differental open circuit voltage decay," *Solid. State. Electron.*, vol. 26, no. 11, pp. 1117–1122, 1983.
[19] T. Kimoto *et al.*, "Nitrogen donors and deep levels in high-quality 4H--SiC epilayers grown by chemical vapor deposition," *Appl. Phys. Lett.*, vol. 67, no. 19, pp. 2833–2835, 1995.
[20] T. Hatakeyama *et al.*, "Measurement of Hall Mobility in 4H-SiC for Improvement of the Accuracy of the Mobility Model in Device Simulation," *Mater. Sci. Forum*, vol. 433–436, pp. 443–446, 2003.
[21] G. Sozzi, M. Puzzanghera, R. Menozzi, and R. Nipoti, "The Role of Defects on Forward Current in 4H-SiC p-i-n Diodes," *IEEE Trans. Electron Devices*, vol. 66, no. 7, pp. 3028–3033, 2019.
[22] K. Danno and T. Kimoto, "Deep level transient spectroscopy on as-grown and electron-irradiated p-type 4H-SiC epilayers," *J. Appl. Phys.*, vol. 101, no. 10, p. 103704, 2007.
[23] P. B. Klein *et al.*, "Lifetime-limiting defects in n- 4H-SiC epilayers," *Appl. Phys. Lett.*, vol. 88, no. 5, p. 52110, 2006.
[24] J. Zhang, L. Storasta, J. P. Bergman, N. T. Son, and E. Janzén, "Electrically active defects in n-type 4H--silicon carbide grown in a vertical hot-wall reactor," *J. Appl. Phys.*, vol. 93, no. 8, pp. 4708–4714, 2003.
[25] R. Nipoti, M. Puzzanghera, G. Sozzi, and R. Menozzi, "Perimeter and Area Components in the I-V Curves of 4H-SiC Vertical p+-i-n Diode With Al+ Ion-Implanted Emitters," *IEEE Trans. Electron Devices*, vol. 65, no. 2, pp. 629–635, 2017.
[26] R. Nipoti, A. Parisini, G. Sozzi, M. Puzzanghera, A. Parisini, and A. Carnera, "Structural and functional characterizations of Al+ implanted 4H-SiC layers and Al+ implanted 4H-SiC pn junctions after 1950° C post implantation annealing," *ECS J. Solid State Sci. Technol.*, vol. 5, no. 10, pp. P621--P626, 2016.
[27] N. T. Son *et al.*, "Negative-U system of carbon vacancy in 4 H-SiC," *Phys. Rev. Lett.*, vol. 109, no. 18, p. 187603, 2012.
[28] L. Lilja, J. Hassan, I. D. Booker, P. Bergman, and E. Janzén, "Influence of growth temperature on carrier lifetime in 4H-SiC epilayers," in *Materials Science Forum*, 2013, vol. 740, pp. 637–640.
[29] R. Nipoti, M. Puzzanghera, and G. Sozzi, "Al + ion implanted 4H-SiC vertical p + -i-n diodes : processing dependence of leakage currents and OCVD carrier lifetimes," *Mater. Sci. Forum*, vol. 897, pp. 439–442, 2017.
[30] T. Kimoto *et al.*, "Carrier lifetime and breakdown phenomena in SiC power device material," *J. Phys. D. Appl. Phys.*, vol. 51, no. 36, p. 363001, 2018.
[31] E. Saito, J. Suda, and T. Kimoto, "Control of carrier lifetime of thick n-type 4H-SiC epilayers by high-temperature Ar annealing," *Appl. Phys. Express*, vol. 9, no. 6, p. 61303, 2016.
[32] S. Yamashita and T. Kimoto, "Analysis of carrier lifetimes in n-type 4H-SiC by rate equations," *Appl. Phys. Express*, 2019.
[33] L. Storasta and H. Tsuchida, "Reduction of traps and improvement of carrier lifetime in 4 H-Si C epilayers by ion implantation," *Appl. Phys. Lett.*, vol. 90, no. 6, p. 62116, 2007.
[34] S. Ichikawa, K. Kawahara, J. Suda, and T. Kimoto, "Carrier recombination in n-type 4H-SiC epilayers with long carrier lifetimes," *Appl. Phys. Express*, vol. 5, no. 10, p. 101301, 2012.
[35] T. Miyazawa, M. Ito, and H. Tsuchida, "Evaluation of long carrier lifetimes in thick 4H silicon carbide epitaxial layers," *Appl. Phys. Lett.*, vol. 97, no. 20, p. 202106, 2010.
[36] B. J. Baliga, *Fundamentals of power semiconductor devices*. Springer Science & Business Media, 2010.
[37] M. Lax, "Cascade capture of electrons in solids," *Phys. Rev.*, vol. 119, no. 5, p. 1502, 1960.
[38] S. Rein, *Lifetime spectroscopy: a method of defect characterization in silicon for photovoltaic applications*, vol. 85. Springer Science & Business Media, 2006.
[39] O. Kordina, J. P. Bergman, C. Hallin, and E. Janzen, "The minority carrier lifetime of n-type 4H-and 6H-SiC epitaxial layers," *Appl. Phys. Lett.*, vol. 69, no. 5, pp. 679–681, 1996.
[40] S. Chowdhury, C. Hitchcock, R. Dahal, I. B. Bhat, and T. P. Chow, "Characteristics of 4H-SiC PiN diodes on lightly doped free-standing substrates," in *2015 IEEE 27th International Symposium on Power Semiconductor Devices & IC's (ISPSD)*, 2015, pp. 353–356.